Diffusion Limited Current Density: A Watershed in Electrodeposition of Lithium Metal Anode

ADVANCED ENERGY MATERIALS
www.advenergymat.de

Diffusion Limited Current Density: A Watershed in Electrodeposition of Lithium Metal Anode

Xieyu Xu, Xingxing Jiao, Olesya O. Kapitanova, Jialin Wang, Valentyn S. Volkov, Yangyang Liu,* and Shizhao Xiong**

Lithium metal is considered to be a promising anode material for high-energy-density rechargeable batteries because of its high theoretical capacity and low reduction potential. Nevertheless, the practical application of Li anodes is challenged by poor cyclic performance and potential safety hazards, which are attributed to non-uniform electrodeposition of Li metal during charging. Herein, diffusion limited current density (DLCD), one of the critical fundamental parameters that govern the electrochemical reaction process, is investigated as the threshold of current density for electrodeposition of Li. The visualization of the concentration field and distribution of Faradic current density reveal how uniform electrodeposition of Li metal anodes can be obtained when the applied current density is below the DLCD of the related electrochemical system. Moreover, the electrodeposition of Li metal within broken solid electrolyte interphases preferentially occurs at the crack spots that are caused by the non-uniform electrodeposition of Li metal. This post-electrodeposition leads to more consumption of active Li when the applied current density is greater than the DLCD. Therefore, lowering the applied current density or increasing the DLCD are proposed as directions for developing advanced strategies to realize uniform electrodeposition of Li metal and stable interfaces, aiming to accelerate the practical application of state-of-the-art Li metal batteries.

1. Introduction

Along with the swift development in the economy and society, the past several decades have witnessed the explosive growth of energy storage demand, especially for the electro-mobile and electronic devices.[1] However, the commercial lithium-ion batteries deliver the limited energy density for the lower specific capacity of graphite anode (372 mA h g^{-1}).[2] Inspired by the near-11-fold higher specific capacity of 3680 mA h g^{-1} and lower reduction potential of −3.04 V versus standard hydrogen electrode, lithium (Li) is regarded as the most promising candidate for anode to pursue the high-energy-density battery systems, including Li—S, Li—O_2, and other rechargeable lithium metal batteries (LMBs).[3] The high exchange current density of Li[4] and the sluggish mass transfer of Li-ion[5] contribute to the mismatch between the supplement of Li-ion and the reduction of Li-ion to form Li-atom, which is the substantial reason for the non-uniform electrodeposition of Li with mossy/dendritic growth.[4,6] The uncontrollable dendritic growth of Li metal can even pierce through the separator to electrically contact with cathode, causing safety hazards. As a consequence, the practical application of Li metal as an anode in LMBs has been hampered for decades.

These days, tremendous endeavor has been devoted to suppressing the non-uniform electrodeposition of dendritic Li, stabilizing the interface with electrolyte, and guaranteeing

X. Xu, O. O. Kapitanova
Department of Materials Science
Lomonosov Moscow State University
Leninskie gory 1, Moscow 119991, Russia
E-mail: olesya.kapitanova@gmail.com

X. Jiao, O. O. Kapitanova, V. S. Volkov, Y. Liu
Center for Photonics and 2D Materials
Moscow Institute of Physics and Technology
9 Institutskiy per., Moscow Region, Dolgoprudny 141701, Russia
E-mail: liuyy0510@hotmail.com

The ORCID identification number(s) for the author(s) of this article can be found under https://doi.org/10.1002/aenm.202200244.

DOI: 10.1002/aenm.202200244

X. Jiao, O. O. Kapitanova, Y. Liu
Autonomous Noncommercial Organization "ID&AS: Inter-Disciplinary & Advanced Studies Center"
Moscow 127495, Russia

J. Wang
State Key Laboratory for Mechanical Behavior of Materials
Xi'an Jiaotong University
Xi'an 710049, P. R. China

S. Xiong
Department of Physics
Chalmers University of Technology
Göteborg SE 412 96, Sweden
E-mail: shizhao.xiong@chalmers.se

the cyclic performance of LMBs.[3a,7] The advanced strategies including optimization of electrolytes like additives and solvent selection,[8] artificial solid electrolyte interphase (SEI) with multifunctional properties,[9] solid-state electrolyte,[10] and functionalized separator,[11] have been reported. These approaches can improve the stability of Li metal anode to a certain extent, which is confirmed by the smooth morphology of cycled Li anode and the prolonged cyclic life. Nevertheless, there still exists a significant gap between the achievements and the demand of practical application, especially for high applied current density and low-fold utilization of Li.[1,12] Therefore, understanding the principle of the electrodeposition of Li metal is essential to create guidelines for developing the strategy specifically.

An important aspect of theoretical investigation on the electrodeposition process of Li metal with density functional theory,[13] molecular dynamics[14] as well as the phase-field simulation has been reported.[15] Among these methods, phase-field simulation is a kind of large-scale computational approach to calculate the change of physical fields and microstructure evolution during the electrochemical reaction process.[16] For example, the local stress and deformation of an SEI layer during Li electrodeposition are investigated to illustrate the impact of structural uniformity and mechanical strength on the stability of the SEI as well as the uniformity of electrodeposition.[17] Also, anisotropic strength, applied voltage, and microstructure of SEI were well discussed to understand the growth mechanism of Li dendrites.[18] Moreover, the exchange current density, a vital parameter to describe the charge-transfer kinetics of the electrochemical reaction, was studied to reveal Faradic current distribution around a dendritic protrusion using Butler–Volmer reaction kinetics.[4] Besides, the concentration gradient is generated during the electrodeposition process of Li onto the substrate, showing the impact of local current density. Due to the high exchange current density, the electrodeposition behavior of Li and local current density is limited by the diffusion of Li-ion from bulk electrolyte to substrate.[19] Specifically, diffusion-limited current density (DLCD) is introduced to describe the current density obtained by maintaining diffusion limitations and ensuring the maximum flux during the electrodeposition reaction.[20] DLCD for electrodeposition of Li is completely controlled by the diffusion rate of the Li-ion, and can be expressed as $j_{lim} = \kappa(c_0 - c_{Li^+})$, where κ is Ilkovic constant, c_{Li^+} is the concentration of Li-ion on a substrate, and c_0 is the concentration of electrolyte. Especially, to pursue the higher energy density with thick cathode and fast-charging process, higher applied current density (ACD) for electrodeposition of Li metal is highly expected. Based on this evidence, DLCD is needed to be investigated to uncover how the ACD affects the electrodeposition of Li and the threshold value for uniform electrodeposition. However, most of the previous reports usually investigated a single factor at a time for the electrodeposition process of Li, and the role of DLCD for mass transfer processes is not well understood. Therefore, a study on the coupling of DLCD and SEI for the mass transfer processes during electrodeposition of Li will reveal new insights on the impact of ACD and structural uniformity of SEI at the same time, which is closer to the experimental environment on Li metal anode.

Herein, the electrodeposition behavior of Li onto rectangle substrate with SEI film under a series of ACD from 0.5 to 3.0 mA cm^{-2} and the evolution of concentration field as well as associated Faradic current density (FAD) were visualized via phase-field simulation based on the Butler–Volmer equation. After relating the electrodeposition uniformity of Li with the ACD and DLCD, it is found that uniform electrodeposition of Li can be realized by the applied current density which is lower the DLCD. Our results show that increasing the DLCD of the related electrochemical system can be a guideline to achieve uniform electrodeposition of Li metal anode with enhanced performance in state-of-the-art LMBs.

2. Results and Discussion

As shown in **Figure 1**a, the diffusion of Li-ions from the bulk electrolyte to the substrate surface and desolvation of Li-ion occur prior to the electrodeposition process of Li. Subsequently, the reduction process of Li-ion can be described according to the simplified reaction:

$$Li^+ + e^- \rightleftharpoons Li \tag{1}$$

The local current density as a function of potential and concentration of Li-ion is given by the Butler–Volmer equation:[18b,19a,21]

$$i = i_0\left[\exp\left(\frac{1.5F}{RT}\eta\right) - \frac{c_{Li^+}}{c_0}\exp\left(-\frac{0.5F}{RT}\eta\right)\right] \tag{2}$$

where i_0 is exchange current density, F is the Faraday constant, R is the ideal gas constant, T is Kelvin temperature, c_{Li^+} is the

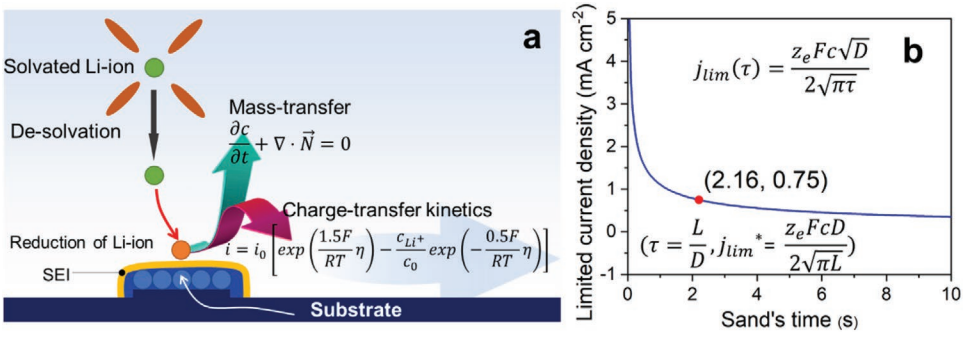

Figure 1. a) Schematic diagram of Li electrodeposition model combining mass-transfer and charge-transfer kinetics. b) Diffusion-limited current density of the electrochemical system in our work.

concentration of Li-ion near the substrate, c_0 is the concentration of Li-ion in bulk electrolyte, and η is overpotential.

Therefore, the boundary conditions can be expressed as:

$$N_{Li^+} \cdot n = -\frac{i_0}{2F}\left[\exp\left(\frac{1.5F\eta}{RT}\right) - \frac{c_{Li^+}}{c_0}\exp\left(-\frac{0.5F\eta}{RT}\right)\right] \quad (3)$$

where N_{Li^+} is the transfer vector in liquid electrolyte and n represents the normal vector of the boundary.

In this model, the ion flux of Li-ion is controlled by the Nernst–Planck equation:[6]

$$N_{Li^+} = -D_{Li^+}\left(\nabla c_{Li^+} - \frac{zFc_{Li^+}}{RT}\nabla\phi\right) \quad (4)$$

where, D_{Li^+} is the diffusion coefficient of Li-ion in a liquid electrolyte, z is the charge of Li-ion, and ϕ is electric potential. Therefore, the mass conservation equation can be expressed as follows:[22]

$$\frac{\partial c_{Li^+}}{\partial t} + \nabla \times N = 0 \quad (5)$$

The concentration equation can be yielded after solving equation (5) with the following boundary conditions of $c_{Li^+}(x,0) = c^*_{Li^+}$, $\lim_{x\to\infty} c_{Li^+}(x,0) = c_0$, $c_{Li^+}(0,0) = 0$, which can be described as

$$c_{Li^+}(x,t) = c^*_{Li^+}\, erf\left(\frac{x}{\sqrt{2D_{Li^+}t}}\right) \quad (6)$$

For the DLCD, a parameter to describe the electrochemical reaction with higher charge-transfer kinetic and controlled by mass transfer is given as

$$j_d(t) = FD_{Li^+}\left[\frac{\partial C_{Li^+}(x,t)}{\partial t}\right]_{x=0} = \frac{FC^*_{Li^+}\sqrt{D_{Li^+}}}{\sqrt{\pi t}} \quad (7)$$

DLCD is employed with Sand's model[23] to explain the effect of ACD on the electrodeposition. In this model, the time for the depletion of Li-ion to zero at electrode surface during the electrodeposition process of Li can be given as $\tau = \frac{L}{D_{Li^+}}$, which is named Sand' time (τ). Here, L is the distance between two electrodes.[20,23] Therefore, after substituting $\tau = \frac{L}{D_{Li^+}}$ for time t in the equation (7), DLCD can be yielded as:

$$j_{lim}{}^* = \frac{z_e FcD_{Li^+}}{2\sqrt{\pi L}} \quad (8)$$

that is ≈0.75 mA cm^{-2} for the electrochemical system studied in this work (Figure 1b).

The phase-field modeling in our work is performed by the finite element method on COMSOL Multiphysics. For the simulation of local current density on Li metal anode, the model's size is 42 × 50 μm^2. In order to yield high-quality results, the model was built by using ultra-fine grid division and the relative error tolerance was set to 1×10^{-5}. The deformation of the grid is considered during the electrodeposition process.

To investigate the electrodeposition of Li onto the substrate with the effect of SEI, an ideal elastic film with a thickness of 1 μm is covered on the rectangles as shown in Figure S1 (Supporting Information). Here, the ideal elastomer is referring to a material that is in accordance with Hooke's law and its deformation is proportional to the external force.[24] The setting up of SEI with characteristics of continuity, uniformity, and isotropy allows this work to focus on the mass transfer process in the electrolyte as well as in SEI and to investigate the relation between ACD and DLCD. The thickness of SEI is set up based on the previous literature about artificial SEI.[25] On the basis of the results in our previous work, the ionic conductivity of SEI film is set as 1% of electrolyte and its modulus is set as 3 GPa.[17b] When a series of current densities from 0.5 to 3.0 mA cm^{-2} are applied, the concentration field near the substrates demonstrates a tendency of non-uniformity, showing the increased concentration gradient (**Figures 2**a–e; Figure S2, Supporting Information). Specifically, the rectangle features are buried in the uneven concentration field and when the current density is increasing to 3.0 mA cm^{-2}, the bottom of space between two rectangles witnesses the ultralow concentration of Li-ion. Based on the non-uniformity of concentration of Li-ion with the increased ACD, the associated Faradic current density (FCD) along the profiles shifts to more uneven. Features on the roof of the rectangle encounter the reinforced FCD with the increase of ACD. Meanwhile, the difference between the roof of the rectangle features and the bottom of the space becomes more apparent.

Moreover, the distribution of FCD along the profile of rectangles when applying different current densities was derived from Figure 2a–e to reveal the further electrodeposition of Li more precisely. As shown in Figure 2f and Figure S3 (Supporting Information), the difference of FCD between the bottom and top increases with the enlarging ACD from 0.5 to 3.0 mA cm^{-2}, illustrating that the difference in the volume of electrodeposited Li can be obtained. It is worth noting that FCD on the middle of the rectangle roof gradually shifts to a lower value than that at the corner with the increase of ACD. The difference of FCD between middle spot and corner spot is –0.031, –0.017, 0.091, 0.15, 0.28 mA cm^{-2} when the ACD varies from 0.5 to 3.0 mA cm^{-2} (Figure 2g), demonstrating that the "tip effect" shows up when ACD is higher than 0.75 mA cm^{-2} and becomes stronger with the increasing ACD. It suggests that the significant concentration gradient created by high ACD changes the distribution of Li-ion concentration as well as FCD near the profile of pillars and triggers the tip effect. Overall, the concentration field and corresponding FCD on the profile of substrate are intimately associated with the current density applied to the electrochemical system.

To quantitatively analyze the effect of ACD on the electrodeposition of Li with the cover of SEI film, the standard deviations of FCD for each calculating step were normalized with that of the first calculating step to illustrate the change of Faradic current density during the electrodeposition process. FCDs on the profile of evaluating morphology during electrodeposition under different ACDs were displayed in **Figure 3**. When ACD ≤ DLCD of 0.75 mA cm^{-2}, the even distribution of FCD shows up in Figure 3a,b. On the contrary, the distribution of FCD is disturbed once the ACD > DLCD and the non-uniformity shifts to a more serious status with the increase of ACD to 3.0 mA cm^{-2} (Figure 3c–e). More specifically, the even distribution of FCD

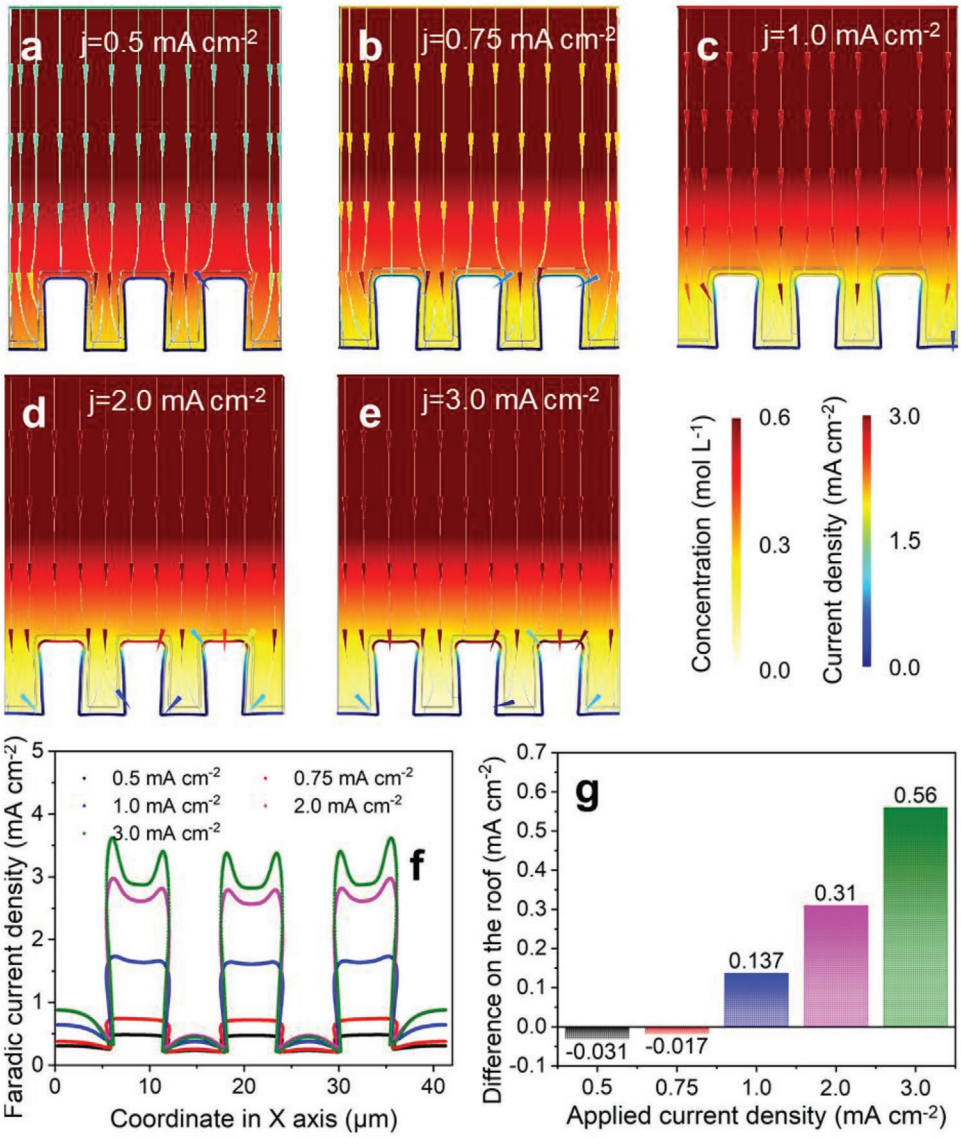

Figure 2. Concentration field (background color) and corresponding electric field (colored lines) near the substrates covered by SEI film with current densities of a) 0.5 mA cm^{-2}, b) 0.75 mA cm^{-2}, c) 1.0 mA cm^{-2}, d) 2.0 mA cm^{-2}, and e) 3.0 mA cm^{-2} at initial state. f) Distribution of Faradic current density at Li–SEI interface under different current densities at initial state. g) Difference of Faradic current densities on the roof of electrodeposited Li.

that realized with lower ACD is stable within whole the electrodeposition process, while the distribution is uneven from the initial to the convergence state with the ACD greater than DLCD. The deterioration degree of the uniformity of FCD distribution is enhanced with the increase of ACD, especially when ACD is greater than DLCD. Quantitatively, the standard deviation of FCD with higher ACD is distinctly greater than that with the ACD lower than DLCD, as seen in Figure 3f and Figure S4 (Supporting Information). The FCD is growing faster with the enlargement of ACD, which suggests the distribution of FCD can be perturbated along with the electrodeposition of Li process and this perturbance is enhanced with the increase of ACD.

The concentration field of Li-ion and corresponding FCD are key parameters for electrodeposition process and thus strongly contribute to the morphology evolution of electrodeposited Li. Owing to the uniform distribution of Li-ion around the rectangle features and the small-difference of FCD, the quasi-equal probability for electrodeposition of Li onto the outside of rectangle features is observed when applying the small current density of 0.5 mA cm^{-2}, facilitating a uniform electrodeposition process (**Figure 4**a). Along with the ACD increases, the distinction of electrodepositing probability at different positions of rectangle features shifts to be more obvious, revealing the uniformity for electrodeposition of Li gradually decays (Figures 4b,c). The final morphology of electrodeposited Li changes from the quasi-rectangle to bulb-like when the ACD grows from 0.5 to 0.75 mA cm^{-2}. Moreover, the features on the roof of "bulb" shows a sunken area when ACD is greater than 0.75 mA cm^{-2} and the sunken area turns to be deeper under the increasing ACD up to 3.0 mA cm^{-2} (Figure 4d,e). With the sunken area, the bulb-like morphology of Li changes to "teeth" like with the enhanced non-uniformity. The morphology evolution of Li

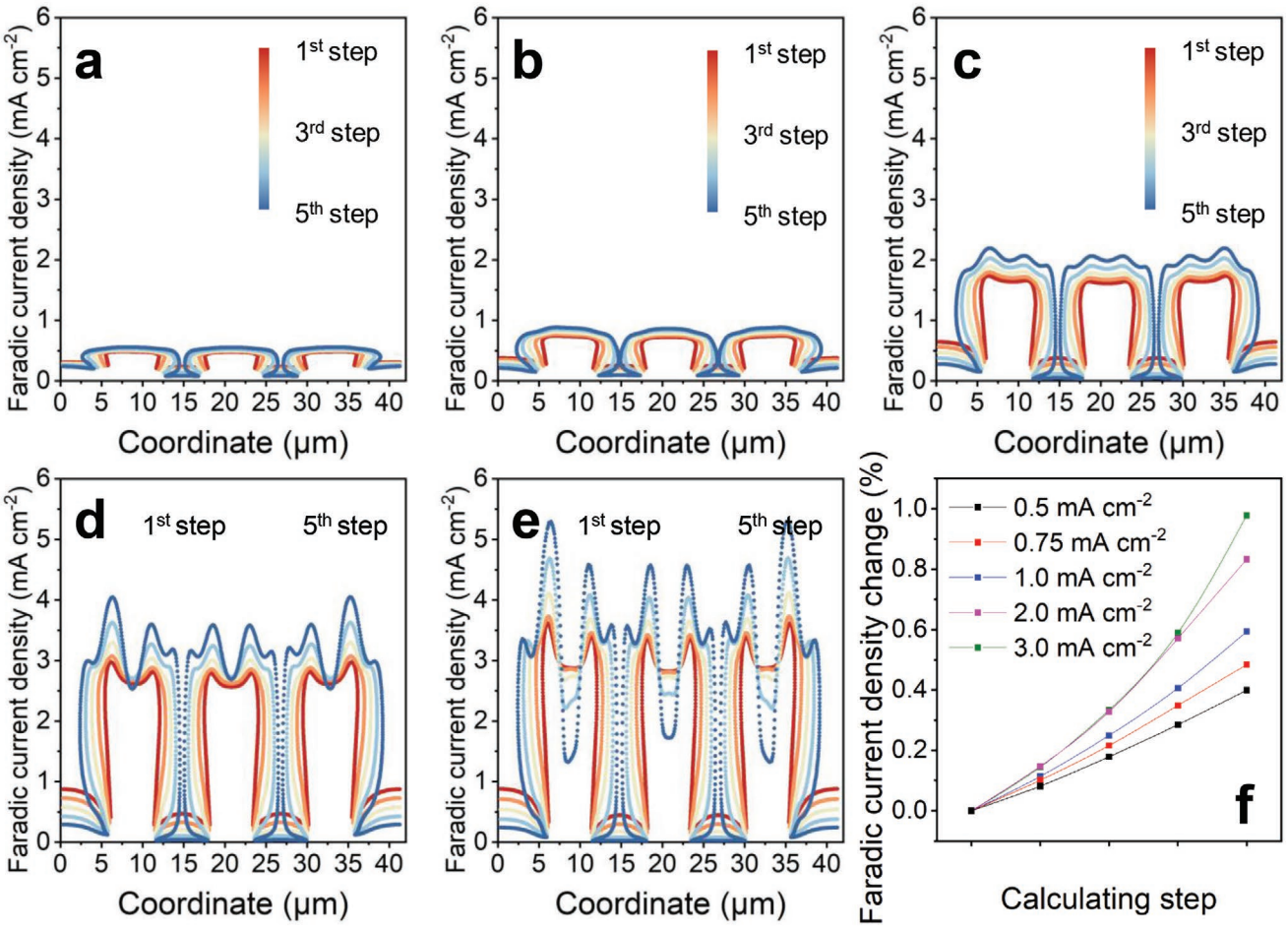

Figure 3. Evolution of Faradic current density on the morphology profile of Li during electrodeposition processing at different applied current density of a) 0.5 mA cm^{-2}, b) 0.75 mA cm^{-2}, c) 1.0 mA cm^{-2}, d) 2.0 mA cm^{-2}, and e) 3.0 mA cm^{-2}. f) Distribution change of Faradic current density on the electrodeposited Li along with the simulating process.

is resulted from the lower FCD at the center of the roof with lower ACD, contributing to the preferable electrodeposition on the vertical direction. Adversely, the higher FCD at the corner induces the faster growth of Li on the local hotspot to form the branched morphology with higher ACD.

To precisely reveal the impact of FCD on the morphological evolution of electrodeposited Li, the index for electrodeposition uniformity of Li at different ACD is defined as the ratio of the electrodepositing rate in *X*-axis to that in *Y*-axis and the schematic diagram is shown in Figure 4f. X_0 and Y_0 are the pristine width and height of rectangle features on the electrode, respectively. The corresponding values are 5 and 10 µm. The uniformity of the electrodeposition of Li is close to unity at lower ACD and drastically decreases when applying higher current densities (Figure 4g). As shown in Figure 4h, the electrodeposition uniformity declines along with an increase in the ratio of ACD to DLCD. When the ratio is smaller than 1 (ACD < DLCD), the uniformity is greater than 1. On the contrary, the uniformity declines to smaller than 1 when the ratio rises to greater than 1. Therefore, DLCD can be regarded as the watershed for the current density that can promote a uniform electrodeposition of Li onto the surface of electrode. Combining with our previous works,[6] we suggest that the depletion rate of Li-ion near the substrate can be postponed when ACD is smaller than DLCD and thus the mismatch between the overfast charge-transfer process and the sluggish mass-transfer process is mitigated to realize the uniform electrodeposition of Li.[5] On the contrary, higher ACD (greater than DLCD) will aggravate the related mismatch and accelerate the depletion of Li-ion, leading to uneven electrodeposition.

This phenomenon can be tracked back to the morphology of electrodeposited Li at convergence state and the concentration of Li-ion under different ACD, as shown in Figure S2 (Supporting Information). The uniformity of concentration distribution is disturbed drastically to generate a severe gradient when ACD is higher than DLCD. Thus, the FCD in *Y*-axis shows a more apparent difference between the top and bottom (Figure S3a,b in Supporting Information). In detail, it shows the fluctuation of FCD on the corner and center of the substrate. The difference of FCD at the corner and that at the center is negative when ACD < DLCD, and shifts to positive when ACD > DLCD (Figure S3c, Supporting Information). Reasonably, the further electrodeposition under SEI with high uniformity can be expected at lower current density and the non-uniformity of electrodeposition is aggravated drastically

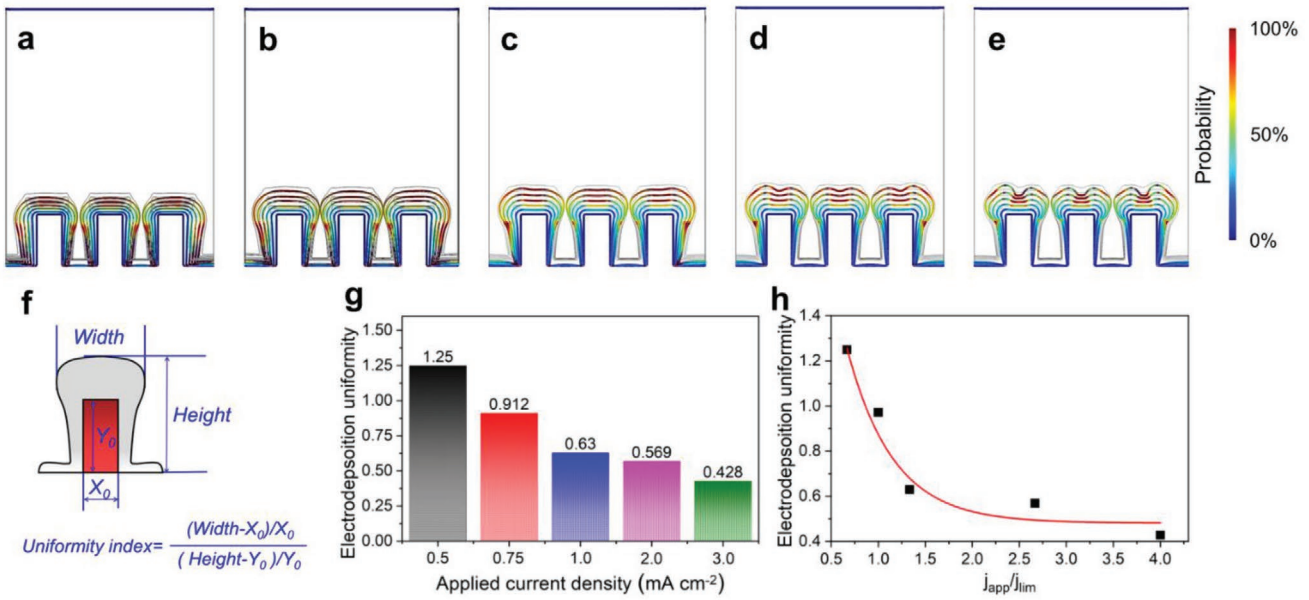

Figure 4. Evolution of Li morphology with electrodeposition probability (colored profile lines) onto substrates at the current density of a) 0.5 mA cm^{-2}, b) 0.75 mA cm^{-2}, c) 1.0 mA cm^{-2}, d) 2.0 mA cm^{-2} and e) 3.0 mA cm^{-2}. f) Schematic diagram for the definition of uniformity index for electrodeposited Li. g) Electrodeposition uniformity under different current densities and h) its dependence on the ratio of applied current density to DLCD.

when applying higher ACD that exceeds the range of DLCD. Experimentally, the stability of electrodeposition of Li at different current densities was confirmed by the steady voltage profiles of Li|Li symmetric cell with over 500 h cycle at a current density of 0.5 mA cm^{-2} and unstable voltage profiles at 3.0 mA cm^{-2} (Figure S5, Supporting Information), demonstrating the reliability of simulation results.

As previously reported, the SEI film on the Li will be broken due to the geometrical fluctuation of the interface caused by the non-uniform electrodeposition.[26] Thus, the broken SEI film on the convergence-state morphology is built to study the post-electrodeposition of Li after the breakage. As shown in Figure S6 (Supporting Information), the position and size of the cracks are set according to the preferred electrodeposited morphology based on the degree of nonuniformity of electrodeposition. The cracks are created on the top corners of bulb-like structures with lower current density and the center of the sunken area at higher current density. Subsequently, the same current densities are applied to track the morphology evolution of electrodeposited Li. At the initial state, the distribution of concentration onto the substrate is uneven with the increase of current density from 0.5 to 3.0 mA cm^{-2} (**Figure 5**a–e). More specifically, the concentration field near the substrate can be divided into two regions: 1) narrow region between two electrodeposited pillars and 2) out-space above the related features. Along with that narrow region between two pillars, the concentration of Li-ion declines with an increase in the ACD and thus the concentration gradient increases from 0.00243 M μm^{-1} at ACD = 0.5 mA cm^{-2} to 0.0158 M μm^{-1} at ACD = 3.0 mA cm^{-2} (Figure 5k; Figure S7, Supporting Information). Different from the concentration distribution situation, the major change of the Faradic current density distribution is revealed near the crack spots. These crack spots are the major terminal of electric streamlines, yielding higher FCD at local area (Figure 5f–j). As shown in Figure 5l, the sharp increase of Faradic current density shows up around the position of $Y > 15$ μm that is near the top of electrodeposits and the tendency is enhanced with increasing applied current density from 0.5 to 2.0 mA cm^{-2}. The maximum Faradic density with ACD = 3.0 mA cm^{-2} is almost the same with that at 2.0 mA cm^{-2}. The increased Faradic current density at the certain position illustrates the preferable electrodeposition on the roof of electrodeposited pillars. It can be expected that Li will be preferentially deposited on the local crack area during the successive electrodeposition process (Figures S8 and S9, Supporting Information).

After successive post-electrodeposition on the local crack, the convergence state of electrodeposited Li shows secondary bulb-like morphology covering the cracks with the current density varying from 0.5 to 1.0 mA cm^{-2} (**Figure 6**a–c). The distribution of Faradic current density on substrate still concentrates at the same spot, as seen in Figure 6f–h. Meanwhile, the post-electrodeposited Li can block the interstice between pillars and leads to the under-concentration region where no electrodeposition can occur, creating a void in the Li microstructure. Thus, our results reveal that the broken SEI also contributes to the improved porosity of Li anode. As shown in Figure 6d,e,i,j, more interfacial fluctuation on the morphology of the post-electrodeposition is observed when ACD > 1.0 mA cm^{-2}, due to the enhanced mismatch between mass-transfer kinetics and charge-transfer kinetics. The dynamic evolution of post-electrodeposition in Figures S8 and S9 (Supporting Information) shows that the post-electrodeposition of Li occurs inside the perforations in advance, and then it grows out of the SEI film. The electrodeposited Li under higher ACD integrates with another neighbor Li microstructure, resulting in the burying of SEI fragments inside Li metal anode as well as exposure of fresh Li toward electrolyte. Therefore, lowering ACD to smaller

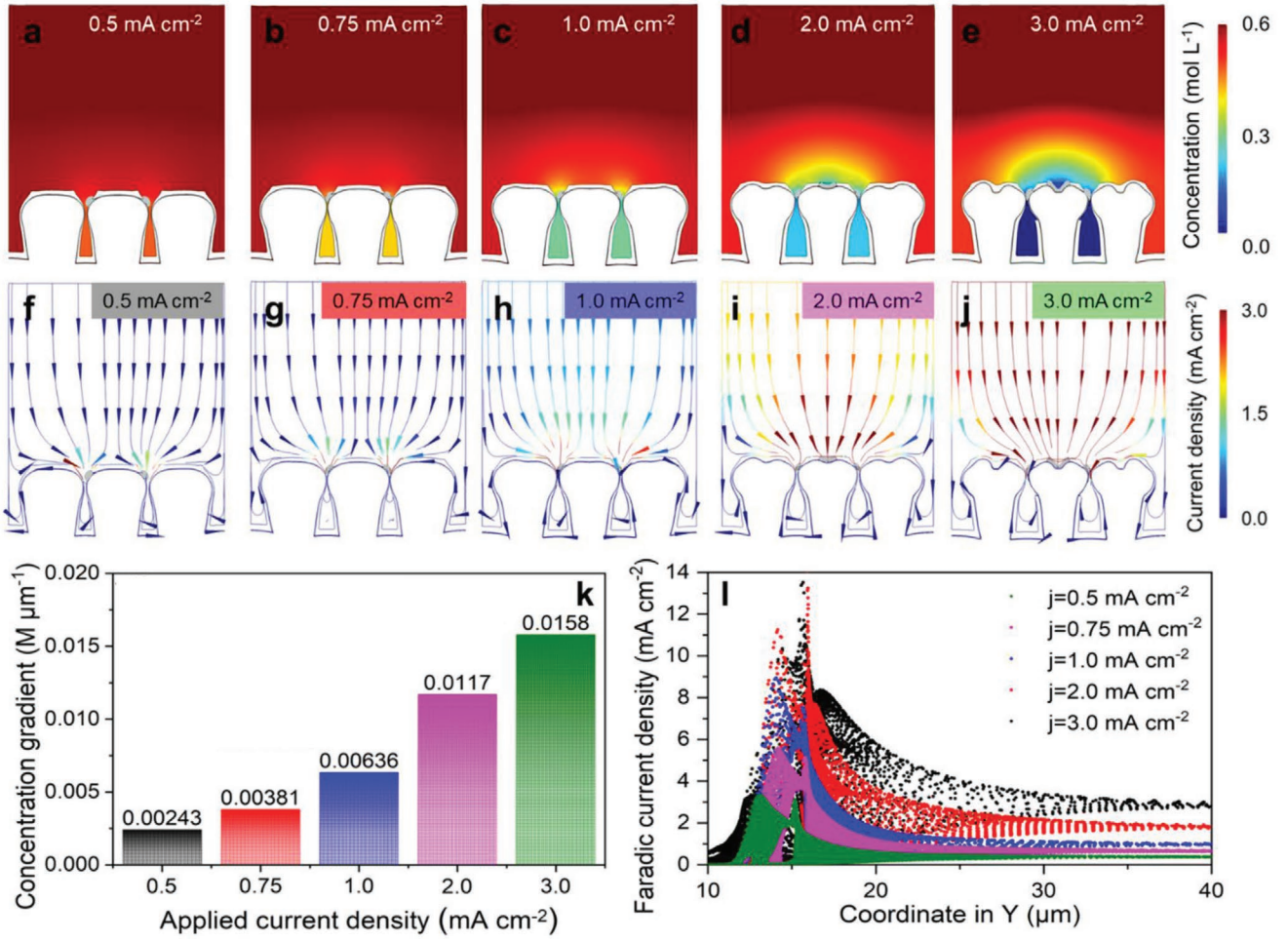

Figure 5. Initial state for electrodeposition of Li within broken SEI film. Concentration field at initial state for electrodeposition of Li covered by broken SEI with applied current density of a) 0.5 mA cm^{-2}, b) 0.75 mA cm^{-2}, c) 1.0 mA cm^{-2}, d) 2.0 mA cm^{-2}, and e) 3.0 mA cm^{-2}. The corresponding electric fields are shown in (f–j). k) Concentration gradient for the electrodeposition of Li with different current densities. l) Distribution of Faradic current density for electrodeposition of Li with different current densities in *Y*-axis. The starting point in *Y*-axis is the ground line of the model shown in Figure S1 (Supporting Information).

than DLCD, not only promotes the uniform electrodeposition of Li and stable cyclic performance, but also promises less consumption of active Li to form new SEI.

The above results indicate that the DLCD is a key parameter for the electrodeposition uniformity of Li, and it is determined by the mass-transfer process of Li-ion near the electrode. Therefore, accelerating the mass transfer of Li-ion to postpone its depletion near Li metal anode can be an effective way to improve the DLCD of the certain electrochemical system. As shown in Equation (8), the charge of Li-ion and Faradic constant are fixed factors and thus the prospects for increasing DLCD can be summarized as follows: i) increasing the concentration of Li-ion in electrolyte, ii) boosting the diffusion of Li-ion near the electrode, such as the design of SEI film with higher ionic conductivity, reducing the dynamic viscosity of electrolyte or improving the operation temperature, iii) lowering the tortuosity of electrode to delay the depletion of Li-ion on electrode. All these practical solutions should be comprehensively considered for obtaining uniform deposition of Li metal anode in rechargeable batteries.

3. Conclusion

To sum up, combining the electrodeposition of Li before and after breakage of SEI at different ACD, we find that the uniform electrodeposition can be achieved when ACD is lower than the DLCD for the certain electrochemical system. On the one hand, the ACD greater than DLCD creates uneven concentration field on the substrate as well as significant difference of FCD on local area, facilitating the preferred electrodeposition of Li at the corner of rectangle feature. On the other hand, the structural-uneven spots on the electrodeposits caused by the lower electrodeposition uniformity will lead to the breakage of SEI. The post-electrodeposited Li with broken SEI grows out of the film and subsequently integrates with the neighbor structure to form void or buried SEI. Therefore, DCLD should be considered as the watershed for uniform electrodeposition of Li, promising a guideline to develop advanced engineering strategies, like increasing the electrochemically active area for lower real ACD or accelerating the diffusion of Li-ion for higher DLCD. Our work paves a

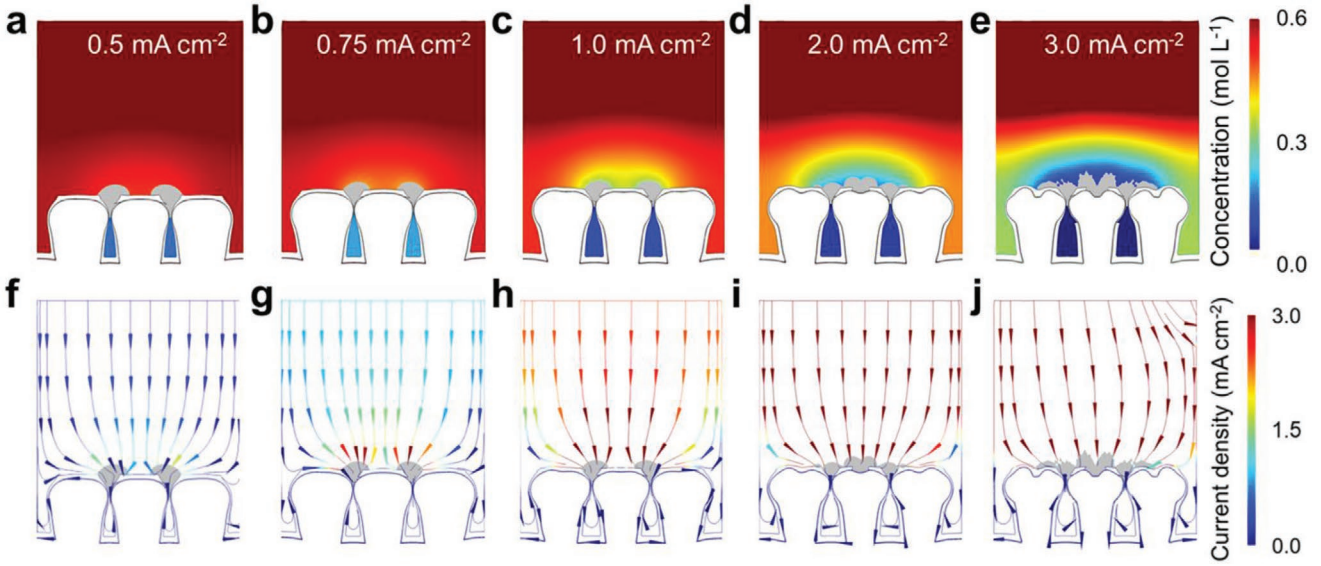

Figure 6. Final state for electrodeposition of Li on broken SEI film. Concentration field at final state for electrodeposition of Li covered by broken SEI with applied current density of a) 0.5 mA cm^{-2}, b) 0.75 mA cm^{-2}, c) 1.0 mA cm^{-2}, d) 2.0 mA cm^{-2}, and e) 3.0 mA cm^{-2}. The corresponding electric field under applied current density of f) 0.5 mA cm^{-2}, g) 0.75 mA cm^{-2}, h) 1.0 mA cm^{-2}, i) 2.0 mA cm^{-2}, and j) 3.0 mA cm^{-2}.

valuable pathway for the practical utilization Li metal anode in high-energy-density batteries.

4. Simulation Section

In this work, it is assumed that the unbroken SEI uniformly and stably attached to Li surface for the modeling in Figures 2–4. The thickness, mechanical properties, and ionic conductivity of SEI here are constant during the electrodeposition process of Li. The unbroken SEI is set as an ideal elastomer before the contact stress between Li metal anode and SEI reaches the stress tolerance limit of the SEI (3.0 GPa). For the broken SEI, it is assumed that the SEI layer damaged when the contact stress exceeds the tolerance limit. The Li at the damaged spot is directly in contact with liquid electrolyte, and the electrochemical reaction at this spot is no longer controlled by SEI.[6,17b]

During the simulation for both models, the efficiency for deposition process is assumed as 100% and the SEI layer as well the Li surface are set as isotropic material. The deposition process of Li ions is described as following steps: i) mass transfer process in liquid electrolyte, ii) mass transfer process in SEI, iii) deposition process on Li surface, iv) generation of extrusion stress and deformation, v) local stress concentration which will break SEI, vi) deposition of Li-ion at broken spot.

The mass transfer flux of Li ion in liquid electrolyte is based on the Nernst-Planck equation:[22a,27]

$$N_L = -D_L \nabla c_L - z u_L F c_L \nabla \varphi_L \tag{9}$$

where N_L is the transfer vector of Li ion in liquid electrolyte, D_L is the diffusion coefficient of Li-ion in liquid electrolyte, c_L is Li-ion concentration, z is the ionic charge of Li-ion, u_L is the ion mobility of Li-ion, F is the Faraday constant, ϕ_L is the liquid electrolyte potential (V).

The mass transfer flux of Li ion in SEI also based on the Nernst-Planck equation:

$$N_{SEI} = -D_{SEI} \nabla c_{SEI} - z u_{SEI} F c_{SEI} \nabla \varphi_{SEI} \tag{10}$$

where N_{SEI} is the transfer vector of Li-ion in SEI, D_{SEI} is the diffusion coefficient of Li-ion in SEI, c_{SEI} is Li-ion concentration, z is the ionic charge of Li-ion, u_{SEI} is the ion mobility of Li-ion in SEI, F is the Faraday constant, ϕ_{SEI} is the SEI partial potential (V).

The deposition process of Li is based on the Butler-Volmer equation, the anode equilibrium potential ϕ_{eq} and overpotential η can be expressed as:

$$\varphi_{eq} = \varphi_0 - \frac{RT}{nF} \ln\left(\frac{1}{c_{\mathrm{Li}^+}}\right)^{\nu_{\mathrm{Li}^+}} \tag{11}$$

$$\eta = \varphi_{anode,0} - \varphi_L - \varphi_{SEI} - \Delta\varphi_{eq} \tag{12}$$

Here, $\phi_{anode,0}$ is the potential of the electrode. Therefore, the local current density on Li surface can be expressed as follows:[18b]

$$i_{lc} = i_0\left(\exp\left(\frac{1.5F\eta}{RT}\right) - \exp\left(\frac{0.5F\eta}{RT}\right)\right) \tag{13}$$

The boundary conditions of the anode are defined as follow:

$$N_{Li^+} \cdot n = -\frac{i_{lc}}{2F} \tag{14}$$

The stoichiometric coefficient of Li-ion in the liquid electrolyte and SEI is $\nu_{Li^+} = -1$, and the stoichiometric coefficient of Li atoms on the electrode is $\nu_{Li^+} = 1$

The extrusion stress between the Li metal and SEI is continuously generated by the deposition of Li and the stress induces

deformation of SEI. The analytical solution of the von Mises stress in the contact area between Li and SEI can be written as a function with respect to the x coordinate:

$$P = \sqrt{\frac{F_u E_c}{2\pi R_c} * \left(1 - \left(\frac{x}{k}\right)^2\right)} \tag{15}$$

$$k = \sqrt{\frac{8F_u R_c}{\pi E_c}} \tag{16}$$

where F_u is the applied load per unit length, E_c is the combined modulus of elasticity, and R_c is the combined radius. The combined radius and combined Young's modulus are defined as follows:[28]

$$E_c = \frac{2E_1E_2}{E_2\left(1-{\nu_1}^2\right) - E_1\left(1-{\nu_2}^2\right)} \tag{17}$$

$$R_C = \lim_{R_2\to\infty} \frac{R_1R_2}{R_1+R_2} = R_1 \tag{18}$$

where E_1 and E_2 are the Young's modulus of Li and SEI, respectively. R_1 is the radius of Li metal pellets. The Poisson's ratio of Li and SEI are ν_1 and ν_2, respectively.

MATLAB and COMSOL Multiphysics were used to analyze the stress distribution at each position in the model. The spot at SEI that exceeds the stress tolerance limit area is excised and imported into a new model for further simulation. The size of the model area is 42×50 μm^2. In order to accurately solve the deformation process of Li and the stress distribution at anode/SEI interface, an ultra-fine mesh with a maximum mesh size of 0.02 microns is used for the grid segmentation of models. Basic parameters for electrolyte used in the modeling are listed in Table S1 (Supporting Information).

5. Experimental Section

The CR2032 type Li|Li symmetric coin cells were assembled to investigate the stability of interface on Li during electrodeposition process under various applied current densities. The electrolyte is 0.56 M Lithium bis(trifluoromethanesulfonyl)imide (LiTFSI, 99.95%, Sigma–Aldrich) in tetra ethylene glycol dimethyl ether (TEGDME, ≥99%, Sigma-Aldrich). Symmetric coin cells were assembled with two Li (200 μm, Chemetall Foote Corp) disks with a diameter of 12 mm, a separator (Celgard@2450) and 40 μL electrolyte. All cells were assembled inside an argon atmosphere glovebox (H_2O < 0.1 ppm, O_2 < 0.1 ppm). The symmetric cells were galvanostatically cycled under current densities from 0.5 to 3.0 mA cm^{-2} on Neware battery testing system.

Supporting Information

Supporting Information is available from the Wiley Online Library or from the author.

Acknowledgements

The authors thank for the support from Chalmers Areas of Advance Materials Science and Energy. This work was financially supported by the National Natural Science Foundation of China (No. 51802256) and China Scholarship Council (No. 201908090043). V.S.V. and O.O.K. acknowledge the support from the Ministry of Science and Higher Education of the Russian Federation (Agreement No. 075-15-2021-606).

Conflict of Interest

The authors declare no conflict of interest.

Author Contributions

X.X. and X.J. contributed equally to this work. X.X. conducted the computing work. X.J. and X.X. performed data analysis. X.J. wrote the manuscript. Both Y.L. and X.X. contributed to the model building. Y.L. and S.X. developed the idea, revised the manuscript, and supervised the project. X.X., X.J., O.O.K., J.W., V.S.V., Y.L., and S.X. reviewed and edited the paper. All authors contributed to the discussions and commented on the paper.

Data Availability Statement

The data that support the findings of this study are available from the corresponding author upon reasonable request.

Keywords

diffusion limited current density, electrodeposition, Li metal anodes, phase-filed modeling, solid electrolyte interphases

Received: January 20, 2022
Revised: February 22, 2022
Published online:

[1] P. Albertus, S. Babinec, S. Litzelman, A. Newman, *Nat. Energy* **2017**, *3*, 16.
[2] M. Winter, B. Barnett, K. Xu, *Chem. Rev.* **2018**, *118*, 11433.
[3] a) D. Lin, Y. Liu, Y. Cui, *Nat. Nanotechnol.* **2017**, *12*, 194; b) J. Xiao, Q. Y. Li, Y. J. Bi, M. Cai, B. Dunn, T. Glossmann, J. Liu, T. Osaka, R. Sugiura, B. B. Wu, J. H. Yang, J. G. Zhang, M. S. Whittingham, *Nat. Energy* **2020**, *5*, 561.
[4] Y. Liu, X. Xu, M. Sadd, O. O. Kapitanova, V. A. Krivchenko, J. Ban, J. Wang, X. Jiao, Z. Song, J. Song, S. Xiong, A. Matic, *Adv. Sci.* **2021**, *8*, 2003301.
[5] J. Xiao, *Science* **2019**, *366*, 426.
[6] X. Xu, Y. Liu, J. Y. Hwang, O. O. Kapitanova, Z. Song, Y. K. Sun, A. Matic, S. Xiong, *Adv. Energy Mater.* **2020**, *10*, 2002390.
[7] H. Li, *Joule* **2019**, *3*, 911.
[8] a) Y. Liu, Y. Pan, J. Ban, T. Li, X. Jiao, X. Hong, K. Xie, J. Song, A. Matic, S. Xiong, *Energy Storage Mater.* **2020**, *25*, 131; b) H. Wang, S. C. Kim, T. Rojas, Y. Zhu, Y. Li, L. Ma, K. Xu, A. T. Ngo, Y. Cui, *J. Am. Chem. Soc.* **2021**, *143*, 2264; c) S. Chen, J. Zheng, L. Yu, X. Ren, M. H. Engelhard, C. Niu, H. Lee, W. Xu, J. Xiao, J. Liu, J.-G. Zhang, *Joule* **2018**, *2*, 1548; d) L. Suo, Y. S. Hu, H. Li, M. Armand, L. Chen, *Nat. Commun.* **2013**, *4*, 1481; e) J. Xie, Z. Liang, Y. C. Lu, *Nat. Mater.* **2020**, *19*, 1006.
[9] a) Y. Sun, M. Amirmaleki, Y. Zhao, C. Zhao, J. Liang, C. Wang, K. R. Adair, J. Li, T. Cui, G. Wang, R. Li, T. Filleter, M. Cai, T. K. Sham, X. Sun, *Adv. Energy Mater.* **2020**, *10*, 2001139; b) S. Ye, L. Wang,

F. Liu, P. Shi, H. Wang, X. Wu, Y. Yu, *Adv. Energy Mater.* **2020**, *10*, 2002647; c) S. J. Tan, J. Yue, X. C. Hu, Z. Z. Shen, W. P. Wang, J. Y. Li, T. T. Zuo, H. Duan, Y. Xiao, Y. X. Yin, R. Wen, Y. G. Guo, *Angew. Chem. Int. Ed. Engl.* **2019**, *58*, 7802; d) Y. Wang, F. Liu, G. Fan, X. Qiu, J. Liu, Z. Yan, K. Zhang, F. Cheng, J. Chen, *J. Am. Chem. Soc.* **2021**, *143*, 2829; e) Y. Zhao, M. Amirmaleki, Q. Sun, C. Zhao, A. Codirenzi, L. V. Goncharova, C. Wang, K. Adair, X. Li, X. Yang, F. Zhao, R. Li, T. Filleter, M. Cai, X. Sun, *Matter* **2019**, *1*, 1215; f) Y. Gao, T. Rojas, K. Wang, S. Liu, D. W. Wang, T. H. Chen, H. Y. Wang, A. T. Ngo, D. H. Wang, *Nat. Energy* **2020**, *5*, 534; g) Y. Y. Liu, X. Y. Xu, X. X. Jiao, L. N. Guo, Z. X. Song, S. Z. Xiong, J. X. Song, *Chem. Eng. J.* **2019**, *371*, 294.

[10] a) S. Xiong, Y. Liu, P. Jankowski, Q. Liu, F. Nitze, K. Xie, J. Song, A. Matic, *Adv. Funct. Mater.* **2020**, *30*, 2001444; b) Q. Liu, Y. Liu, X. Jiao, Z. Song, M. Sadd, X. Xu, A. Matic, S. Xiong, J. Song, *Energy Storage Mater.* **2019**, *23*, 105; c) Q. Zhao, X. Liu, S. Stalin, K. Khan, L. A. Archer, *Nat. Energy* **2019**, *4*, 365; d) T. Dong, J. Zhang, G. Xu, J. Chai, H. Du, L. Wang, H. Wen, X. Zang, A. Du, Q. Jia, X. Zhou, G. Cui, *Energy Environ. Sci.* **2018**, *11*, 1197.

[11] a) Y. Liu, S. Xiong, J. Wang, X. Jiao, S. Li, C. Zhang, Z. Song, J. Song, *Energy Storage Mater.* **2019**, *19*, 24; b) H. Lee, X. Ren, C. Niu, L. Yu, M. H. Engelhard, I. Cho, M.-H. Ryou, H. S. Jin, H.-T. Kim, J. Liu, W. Xu, J.-G. Zhang, *Adv. Funct. Mater.* **2017**, *27*, 1704391; c) Y. Liu, Q. Liu, L. Xin, Y. Liu, F. Yang, E. A. Stach, J. Xie, *Nat. Energy* **2017**, *2*, 17083.

[12] J. Liu, Z. Bao, Y. Cui, E. J. Dufek, J. B. Goodenough, P. Khalifah, Q. Y. Li, B. Y. Liaw, P. Liu, A. Manthiram, Y. S. Meng, V. R. Subramanian, M. F. Toney, V. V. Viswanathan, M. S. Whittingham, J. Xiao, W. Xu, J. H. Yang, X. Q. Yang, J. G. Zhang, *Nat. Energy* **2019**, *4*, 180.

[13] a) C. T. Yang, Y. Qi, *Chem. Mater.* **2021**, *33*, 2814; b) D. Gaissmaier, D. Fantauzzi, T. Jacob, *J. Chem. Phys.* **2019**, *150*, 041723.

[14] a) A. Hagopian, M. L. Doublet, J. S. Filhol, *Energy Environ. Sci.* **2020**, *13*, 5186; b) Y. Li, K. Leung, Y. Qi, *Acc. Chem. Res.* **2016**, *49*, 2363; c) A. Aryanfar, T. Cheng, A. J. Colussi, B. V. Merinov, W. A. GoddardIII, M. R. Hoffmann, *J. Chem. Phys.* **2015**, *143*, 134701.

[15] P. Zou, Y. Sui, H. Zhan, C. Wang, H. L. Xin, H. M. Cheng, F. Kang, C. Yang, *Chem. Rev.* **2021**, *121*, 5986.

[16] a) Q. Wang, G. Zhang, Y. Li, Z. Hong, D. Wang, S. Shi, *npj Comput. Mater.* **2020**, *6*, 176; b) A. Mistry, A. A. Franco, S. J. Cooper, S. A. Roberts, V. Viswanathan, *ACS Energy Lett.* **2021**, *6*, 1422.

[17] a) X. Shen, R. Zhang, X. Chen, X. B. Cheng, X. Li, Q. Zhang, *Adv. Energy Mater.* **2020**, *10*, 1903645; b) Y. Liu, X. Xu, O. O. Kapitanova, P. V. Evdokimov, Z. Song, A. Matic, S. Xiong, *Adv. Energy Mater.* **2022**, *12*, 2103589.

[18] a) W. Mu, X. Liu, Z. Wen, L. Liu, *J. Energy Storage* **2019**, *26*, 100921; b) L. Chen, H. W. Zhang, L. Y. Liang, Z. Liu, Y. Qi, P. Lu, J. Chen, L. Q. Chen, *J. Power Sources* **2015**, *300*, 376.

[19] a) R. Akolkar, *J. Power Sources* **2013**, *232*, 23; b) M. A. Vorotyntsev, M. D. Levi, A. Schechter, D. Aurbach, *J. Phys. Chem. B* **2001**, *105*, 188; c) Y. Lee, B. Ma, P. Bai, *Energy Environ. Sci.* **2020**, *13*, 3504.

[20] P. Bai, J. Li, F. R. Brushett, M. Z. Bazant, *Energy Environ. Sci.* **2016**, *9*, 3221.

[21] Y. Okajima, Y. Shibuta, T. Suzuki, *Comput. Mater. Sci.* **2010**, *50*, 118.

[22] a) L. Clarance Mary, *Int. J. Electrochem. Sci.* **2021**, *16*, 151037; b) T. T. Vu, G. H. Eom, J. Lee, M. S. Park, J. Moon, *J. Power Sources* **2021**, *496*, 229791.

[23] H. J. S. Sand, *Philos. Mag.* **1901**, *1*, 45.

[24] A. L. King, *Am. J. Phys.* **1946**, *14*, 28.

[25] a) R. G. Fedorov, S. Maletti, C. Heubner, A. Michaelis, Y. Ein-Eli, *Adv. Energy Mater.* **2021**, *11*, 2101173; b) S. Gao, F. Sun, N. Liu, H. Yang, P. F. Cao, *Mater. Today* **2020**, *40*, 140; c) R. Xu, X. B. Cheng, C. Yan, X. Q. Zhang, Y. Xiao, C. Z. Zhao, J. Q. Huang, Q. Zhang, *Matter* **2019**, *1*, 317.

[26] S. Xiong, K. Xie, Y. Diao, X. Hong, *J. Power Sources* **2014**, *246*, 840.

[27] M. Rosso, C. Brissot, A. Teyssot, M. Dollé, L. Sannier, J. M. Tarascon, R. Bouchet, S. Lascaud, *Electrochim. Acta* **2006**, *51*, 5334.

[28] a) M. Zang, W. Gao, Z. Lei, *Comput. Mech.* **2011**, *48*, 541; b) A. Sharma, R. L. Jackson, *Tribol. Lett.* **2017**, *65*, 112.